Acta Crystallographica Section A
Foundations of Crystallography
ISSN 0108-7673

Received 23 June 2006
Accepted 18 January 2007

Phase and amplitude recovery and diffraction image generation method: structure of Sb/Au(110)–$\sqrt{3} \times \sqrt{3}$R54.7° from surface X-ray diffraction

R. Fung, V. L. Shneerson, P. F. Lyman, S. S. Parihar, H. T. Johnson-Steigelman and D. K. Saldin*

Department of Physics and Laboratory for Surface Studies, University of Wisconsin-Milwaukee, PO Box 413, Milwaukee, WI 53201, USA. Correspondence e-mail: dksaldin@uwm.edu

The discovery that the phase problem of diffraction from non-periodic objects may be solved by *oversampling* the diffraction intensities in reciprocal space with respect to a Nyquist criterion has opened up new vistas for structure determination by diffraction methods. A similar principle may be applied to the problem of surface X-ray diffraction (SXRD), where, owing to the breaking of a crystal periodicity normal to its surface, diffraction data consist of a set of superstructure rods (SRs) due to scattering from the parts of the surface whose structure is different from that of the truncated bulk and of crystal truncation rods (CTRs), formed by interfering contributions from the surface and the bulk. A phase and amplitude recovery and diffraction image generation method (PARADIGM) is described that provides a prescription for finding the unmeasured amplitudes and phases of the surface contributions to the CTRs in addition to the phases of the SRs, directly from the diffraction data. The resulting 'diffraction image' is the basis of a determination of the previously unknown multidomain structure of Sb/Au(110)–$\sqrt{3} \times \sqrt{3}$R54.7°.

1. Introduction

Owing to the relatively deep penetration of X-rays into a sample, the systematic use of X-rays for the study of surfaces did not occur until relatively recently (Andrews & Cowley, 1985; Robinson, 1986), with the development of the technique of surface X-ray diffraction (SXRD). Unlike the case of the crystallography of bulk samples, where X-rays are scattered into particular directions specified by reciprocal-lattice points, the distribution of scattered X-rays in SXRD forms a set of rods in reciprocal space, known as crystal truncation rods (CTRs), which have both surface and bulk contributions, and superstructure rods (SRs) which arise purely from the surface. The relative dispositions of CTRs and SRs give an indication of the relative configurations of the surface and bulk unit cells. An analysis of the distribution of measured intensities along these diffraction rods can give detailed information about the atomic scale structure of the sample.

Since it is straightforward to calculate the intensity distributions of CTRs and SRs for a given model of a crystal surface, the usual method of determining a surface structure is by repeated comparisons of simulated SXRD data with experiment for a series of model structures. The degree of the fit between simulation and experiment is determined by an objective measure of discrepancy, *e.g.* a χ^2 value of a least-squares fit. In this conventional, trial-and-error, method, the correct structure is taken as the one that minimizes the measure of discrepancy. If a good guess can be made of the approximate structure, it is possible to automate the refinement of a number of parameters, such as the positions and occupancies of the atoms in the postulated structure, the vibrational amplitudes, the relative abundances of each of the symmetry-related domains and parameters characterizing the roughness of the surface (Vlieg, 2000).

However, owing to an almost unlimited number of possible starting models, there is no guarantee that an appropriate one may be guessed that will refine to the correct structure. Thus, there is a need for the development of a general method of extracting, directly from the measured data, at least an approximation to the electron density of the unknown surface unit cell that can suggest a suitable initial model.

In the crystallography of bulk samples, the square roots of the measured intensities of Bragg spots are proportional to the amplitudes of Fourier coefficients of the electron density of the unit cell. An approximation to that electron density may be found by an inverse Fourier transform if approximate phases may be assigned to each of these Fourier coefficients. In protein crystallography, the three most commonly used methods for assigning these phases are ones that require extra experimental measurements, as in the techniques of multiple isomorphous replacement (MIR) (Green *et al.*, 1954; Blow & Crick, 1959) and multiwavelength anomalous dispersion (MAD) (Hendrickson, 1991; Leahy *et al.*, 1992); or by identification of a known structure similar to the one being sought,

as in the technique of molecular replacement (Rossmann & Blow, 1962).

For crystals with a smaller number of atoms per unit cell, techniques have been developed that do not require such extra experimental data. They are known collectively as direct methods (Woolfson, 1961; Giacovazzo, 1980) and exploit extra relations between measured scattered amplitudes and unknown phases arising from restrictions on the form of the electron density due to its reality, positivity and atomicity, to estimate these phases by purely theoretical arguments. Initial estimates of the phases are usually refined by an iterative process of *density modification* (see *e.g.* Drenth, 1994) that alternately satisfies constraints in real and reciprocal space and has been termed Fourier recycling. More recently, Oszlányi & Sütő (2004) have suggested an *ab initio* method of phasing high-resolution X-ray crystallographic data from small molecules by a form of Fourier recycling that involves charge flipping in real space. As pointed out by Millane (1990), these approaches are closely analogous to methods of phase retrieval in optics. In crystallography, the aim of such methods is to find an electron density of sufficiently high quality to enable the building of an initial atomistic model of the structure. The latter may be refined by a χ^2 fit to the data.

It was shown by Saldin *et al.* (Saldin, Harder, Shneerson & Moritz, 2001; Saldin, Harder, Vogler *et al.*, 2001) that the electron density of a surface may be recovered from SXRD data by a Fourier recycling method together with information about the crystal structure of the bulk of the material. The former work involved a modification of the real-space surface electron density at each iteration by the 'maximum-entropy' prescription of Collins (1982), while the latter applied a positivity constraint to the recovered electron density.

Recently, such an algorithm was successfully applied to the recovery of the surface electron density of clean Au(110) (Lyman *et al.*, 2005) and Sb-covered Au(110) from experimental data. When covered by Sb adatoms, the Au(110) face successively exhibits several different surface reconstructions. Using low-energy electron diffraction (LEED), we found (in the Wood notation, see below) a $c(2\times 2)$, a $(\sqrt{3}\times\sqrt{3})$ R54.7°, and a $p(5\times 6)$ phase at Sb coverages of about $\frac{1}{2}$, $\frac{2}{3}$ and >1 monolayer, respectively. These phases had not been reported in the literature before. We have measured SXRD data for these three phases. The use of our direct method for the determination of the structure of the $c(2\times 2)$ phase is published elsewhere (Lyman *et al.*, 2006). We are currently investigating the structure of the $p(5\times 6)$ phase. The present paper describes the determination of the structure of the $(\sqrt{3}\times\sqrt{3})$ R54.7° phase with coverage $\theta_{\rm Sb}=\frac{2}{3}$. In these applications to experimental data, the real-space electron density was made to satisfy a *support constraint* (Fienup, 1978; Miao *et al.*, 1999) at each iteration.

The plan of the paper is as follows: first we discuss what may be deduced about the structure from an observation of the pattern of the so-called 'in-plane' Bragg reflections. We will see that this pattern can arise from the superposition of diffraction patterns from four symmetrically related domains of $(\sqrt{3}\times\sqrt{3})$ surface superstructures. As a first step towards the determination of the internal structure of the $(\sqrt{3}\times\sqrt{3})$ surface unit cells, we calculate a 'partial' Patterson function from the intensities of the superstructure diffraction rods. We point out that this function does not contain enough information to distinguish between alternative models. Next, we determine an approximate electron-density map of the surface unit cell by our direct method applied to the measured data. This immediately suggests a model in which two diagonal rows of Sb adatoms alternate with a row of Au adatoms, all adatoms residing in hollow sites on the surface. Lastly, we apply a conventional refinement method for the final structure solution.

2. Diffraction conditions

The aim of surface X-ray diffraction is to determine the atomic scale structure of the outermost few atomic layers on a surface. The structure of the deeper atomic layers is not the primary target of investigation – rather, it is usually assumed known. A crystalline sample may be regarded as periodic in the plane parallel to the surface, but of course any periodicity perpendicular to the surface is broken by the very existence of the surface. Nevertheless, the relative atom positions in the surface may be specified by a coordinate system of two unit vectors (say $\mathbf{a}_1$ and $\mathbf{a}_2$) of the bulk lattice parallel to the surface) and one (say $\mathbf{a}_3$) equal to a lattice vector of the bulk in a direction perpendicular to the surface. A set of basis vectors $\{\mathbf{A}\}$ of the reciprocal lattice is defined in terms of these real-space basis vectors $\{\mathbf{a}\}$ *via*

$$\mathbf{a}_i\cdot\mathbf{A}_j=\delta_{ij}. \tag{1}$$

The significance of the basis vectors $\{\mathbf{A}\}$ is that the complex scattered amplitude

$$F_{\mathbf{q}}=|F_{\mathbf{q}}|\exp(i\phi_{\mathbf{q}}) \tag{2}$$

from a repeat unit of the surface (the surface structure factor) may be regarded as a function of the reciprocal-space scattering vector $\mathbf{q}$ defined in terms of the basis vectors $\{\mathbf{A}\}$ by

$$\mathbf{q}=h\mathbf{A}_1+k\mathbf{A}_2+l\mathbf{A}_3, \tag{3}$$

where (hkl) are a set of Laue indices.

With this definition of Laue indices, it follows that Bragg diffraction conditions will permit non-zero values of $F_{\mathbf{q}}$ only for scattering vectors $\mathbf{q}$ specified by integer values of Laue indices h and k if the lateral periodicity is the same as that of the bulk, and by specific fractional values of either or both of these indices if the surface unit cell is larger than (but still commensurate with) the bulk unit cell. As for the third Laue index, the breaking of the periodicity in the direction normal to the surface removes any restriction on the values of l for permitted scattering vectors. Thus, non-zero values of $F_{\mathbf{q}}$ are found along a set of *rods* in reciprocal space parallel to $\mathbf{A}_3$. Those corresponding to integer values of h and k (which have scattering contributions from the bulk of the crystal as well as the surface) are the CTRs and those specified by fractional values of either h or k (which arise solely from scattering by the surface region) are the SRs.

3. Experiment

Prior to analysis by SXRD, initial experiments were carried out at the University of Wisconsin–Milwaukee to establish the symmetries induced by Sb adsorption (using low-energy electron diffraction, LEED) and to correlate the Sb coverage with each of the observed phases (using X-ray photoelectron spectroscopy, XPS). XPS analysis (Seah, 1983) from samples exhibiting a $(\sqrt{3} \times \sqrt{3})$ LEED pattern (not shown) yielded an Sb coverage of 0.8 ± 0.15 ML (ML = monolayer, 1 ML = 8.5×10^{14} atoms cm^{-2}), with no impurity species present. Details of the analysis have been published elsewhere (Lyman *et al.*, 2006). The exact Sb coverage of the surface for which an extensive SXRD data set was collected was not accurately determined due to the lack of an XPS facility in the SXRD endchamber.

Quantitative structural measurements were made using SXRD at beamline X22C at the National Synchrotron Light Source (NSLS) at the Brookhaven National Laboratory. The X22C endstation (Gibbs *et al.*, 1990) is equipped with a 6-circle diffractometer for SXRD measurements, and an UHV chamber with a cylindrical mirror analyzer for Auger electron spectroscopy.

The electropolished Au(110) single crystal had a bulk mosaic spread of $<0.04^\circ$. Its surface was cleaned by standard Ar^+ sputtering and annealing cycles, whereupon it exhibited the well known (2×1) reconstruction (Moritz & Wolf, 1979). Monolayer quantities of Sb (99.9999% purity) were then deposited from an effusion cell operated at 680 K. The sample temperature was monitored using a W–WRe thermocouple attached directly to the sample. Both deposition onto a RT substrate with post-annealing to 700 K and deposition onto a substrate held at 700 K were investigated. In either case, the samples were typically held at 700 K for 5 min after deposition ceased, and then slowly cooled. This annealing temperature is near the $(2 \times 1) \rightarrow (1 \times 1)$ deconstruction temperature (735 K) (Keane *et al.*, 1991; Sprösser *et al.*, 1991) and above the Sb:Au eutectic temperature (630 K) (Moffat, 1986; Chevalier, 1989), but below the temperature at which the clean surface roughens (∼784 K) (Keane *et al.*, 1991). Thus, the surface system had sufficient mobility and thermal activation to reach its quasi-equilibrium RT state upon slow cooling.

Radiation of 10.8 keV was used to acquire the SXRD data. Since we are considering a (110) surface, it is convenient to define a unit cell of the bulk in terms of two unit vectors parallel to the surface, a third perpendicular to it. Thus, it is convenient to define a real-space bulk unit cell by the unit vectors $\mathbf{a}_1 = \frac{1}{2}[\bar{1}10]_{\rm cub}$ and $\mathbf{a}_2 = [001]_{\rm cub}$, parallel to the surface, and $\mathbf{a}_3 = \frac{1}{2}[110]_{\rm cub}$, perpendicular to it, where the subscript refers to the conventional f.c.c. cell. For Au, the magnitudes of these bulk unit vectors are 2.88, 4.07 and 2.88 Å, respectively. By equation (1), the reciprocal-space coordinate system may be specified by $\mathbf{A}_1 = (\bar{1}10)_{\rm cub}$, $\mathbf{A}_2 = (001)_{\rm cub}$ and $\mathbf{A}_3 = (110)_{\rm cub}$. In this frame, the index l refers to momentum transfer $q_\perp$ perpendicular to the surface plane, while the indices h and k refer to in-plane momentum transfer $q_\parallel$. The angle of incidence was kept equal to the exit angle to allow access to relatively large values ($\simeq 4$ Å^{-1}) of $q_\perp$, while still accessing up to $q_\parallel \simeq 10$ Å^{-1}. The measured structure factors were corrected (Vlieg, 1997) for geometrical and polarization effects. Approximately 3050 surface structure-factor amplitudes were measured, covering 1228 non-equivalent reflections distributed along 88 (hk) rods. In terms of the Laue indices, this encompassed the range $0 \leq h \leq 4$, $0 \leq k \leq 4$ and $0 \leq l \leq 1.8$. Both CTRs and SRs were recorded over this range. The measured intensity variations of a couple of typical CTRs and SRs and their estimated errors are denoted by the vertical bars in Figs. 1 and 2, respectively.

4. Surface unit cell from 'in-plane' diffraction pattern

Owing to the breaking of translational symmetry normal to a surface, a surface unit cell may be defined by just two unit vectors, $\mathbf{b}_1$ and $\mathbf{b}_2$, with directions parallel to the surface. In general, due to the presence of adsorbates, or of surface reconstruction, these vectors may differ from the corresponding vectors $\mathbf{a}_1$ and $\mathbf{a}_2$ of the bulk. Since the

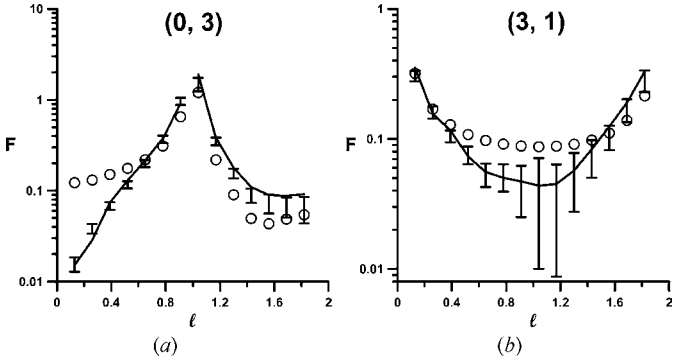

Figure 1
Two sample crystal truncation rods (CTRs) with (h, k) Laue indices (0, 3) and (3, 1). The measured data and their errors are denoted by the vertical bars. The ordinate is specified by a logarithmic scale. The open circles represent the fits to this data by the PARADIGM. The best fit from a conventional atomic model based refinement with the ROD program (Vlieg, 2000) is indicated by the solid line.

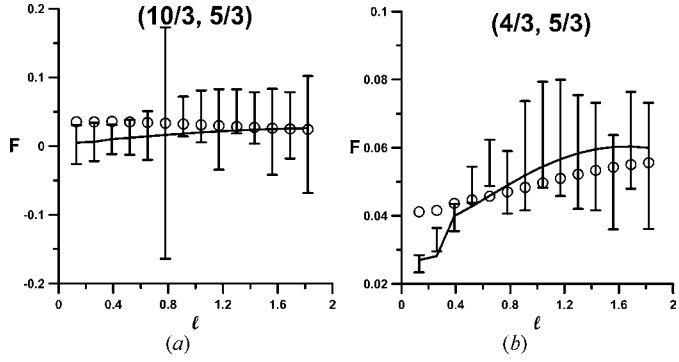

Figure 2
Two sample superstructure rods (SRs) with (h, k) Laue indices (10/3, 5/3) and (4/3, 5/3). The measured data and their errors are denoted by the vertical bars. The open circles represent the fits to this data by the PARADIGM. The best fit from a conventional atomic model based refinement with the ROD program (Vlieg, 2000) is indicated by the solid line.

corresponding surface and bulk vectors may differ, not only in magnitude but also in direction, the most general relationship between these vectors may be specified by a (2×2) matrix. However, in cases where the angles between $\mathbf{b}_1$ and $\mathbf{a}_1$ on the one hand, and between $\mathbf{b}_2$ and $\mathbf{a}_2$ on the other, are equal, a more transparent convention, known as the Wood notation, is more commonly used. Since, for the surface structure studied here these conditions hold, we specify our surface by the version of the Wood notation (Wood, 1964) in which a surface structure is specified by the general formula

$$A/S(hkl) - i\left(\frac{b_1}{a_1} \times \frac{b_2}{a_2}\right)R\alpha, \qquad (4)$$

where A represents the chemical formula of any overlayer, S that of the substrate, (hkl) specify Miller indices of the substrate surface, i may take the values p for a primitive, or c for a centered overlayer unit cell, b_1 and b_2 are magnitudes of the surface unit vectors, and a_1 and a_2 those of the corresponding bulk unit vectors. In the same formula, $R\alpha$ indicates a rotation through an angle α of the surface unit cell with respect to the bulk unit cell. In this notation, $A/$ is dropped if there is no overlayer, and the symbol i is often dropped for a primitive surface unit cell.

Non-zero diffraction intensities were found along rods with in-plane Laue indices $h = \frac{m}{3}$ and $k = \frac{n}{3}$, where m and n are both integers, and h and k are either both integers (CTRs) or both non-integers (SRs). Fig. 3 is a schematic diagram of the observed in-plane diffraction pattern (*i.e.* that corresponding to $l = 0$). The diffraction intensities were observed to have the same *p2mm* symmetry as the Au bulk. This diffraction pattern is consistent with a surface reconstruction in which the surface unit cells are similar rectangles to that of the bulk unit cell, but $\sqrt{3}$ times larger in linear dimensions and rotated by 54.7° relative to the latter [hence the specification of the surface in the full Wood notation (4) as Sb/Au(110)–$(\sqrt{3} \times \sqrt{3})R54.7°$]. Half of the superstructure reflections (Fig. 3, unfilled circles with thick outline) can be accounted for by having domains (type 1) in which the surface lattice vectors are rotated 54.7° clockwise from the bulk lattice vectors (Fig. 4); the other half (Fig. 3, unfilled circles with thin outline), requires domains (type 2) in which the rotation is in the counterclockwise sense. Features in such surface unit cells line up to form rows parallel to one of the two diagonals of the bulk unit cells (Fig. 5).

An alternative way to describe the reconstruction is to have rectangular surface unit cells with the size and orientation of a (3×3) array of bulk unit cells (Fig. 4). Reconstruction with such surface unit cells, in general, produces non-zero diffraction intensities for all reflections with in-plane Laue indices $h = \frac{m}{3}$ and $k = \frac{n}{3}$, where m and n are both integers. CTR reflections have integer values for both h and k; whereas SR reflections have non-integer values for either or both of the in-

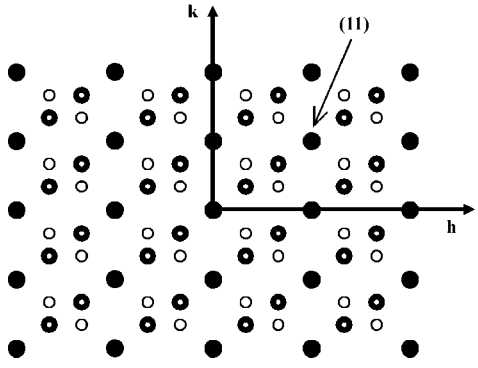

Figure 3
Schematic diagram of our observed diffraction pattern. Filled and unfilled circles denote crystal truncation rod (CTR) and superstructure rod (SR) reflections, respectively. Unfilled circles with thick and thin outlines represent SR reflections arising from surface domains with different orientations. The two types of surface domains are referred to as type 1 (thick outline) and type 2 (thin outline) in the main text.

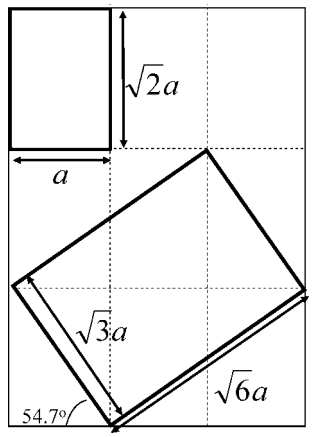

Figure 4
Real-space unit cells. The rectangle at the top left corner with dimensions $a \times \sqrt{2}a$ represents a bulk unit cell. The rotated rectangle with dimensions $\sqrt{3}a \times \sqrt{6}a$ is a type-1 $(\sqrt{3} \times \sqrt{3})$ surface unit cell. Its sides make angles 54.7° with those of the bulk unit cell. Finally, the (3×3) surface unit cell has the size and orientation of a (3×3) array of bulk unit cells.

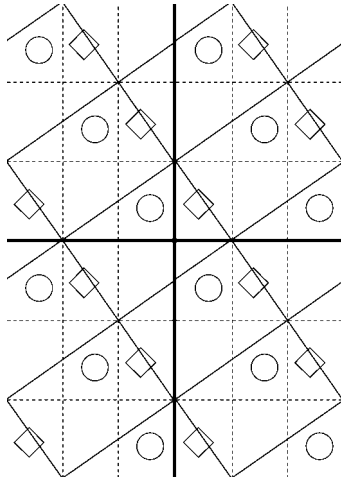

Figure 5
Real-space features that are consistent with the observed diffraction pattern line up to form rows parallel to one of the two diagonals of the bulk unit cells. The arrangement shown here is referred to as type 1 in the main text.

plane Laue indices. For this general (3×3) diffraction pattern to reduce to the one observed experimentally, certain *extinction* conditions must be met. These conditions arise for the following reasons: as pointed out before, the contents of the (3×3) surface unit cell in real space must be such that features form rows parallel to one of the two diagonals of the bulk unit cells, resulting in the same arrangement as in the previous $(\sqrt{3} \times \sqrt{3})$ description (Fig. 4). If only type-1 surface unit cells are present (Fig. 5), the surface structure factor of reflection (hkl) takes the form

$$\begin{aligned} S_{(hkl)} = \sum_j f_j \big(& \exp[2\pi i(hx_j + ky_j + lz_j)] \\ & + \exp\{2\pi i[h(x_j + 1) + k(y_j - 1) + lz_j]\} \\ & + \exp\{2\pi i[h(x_j + 2) + k(y_j - 2) + lz_j]\}\big) \\ = & \{1 + \exp[2\pi i(h - k)] + \exp[2\pi i(2h - 2k)]\} \\ & \times \sum_j f_j \exp[2\pi i(hx_j + ky_j + lz_j)], \end{aligned} \tag{5}$$

where the sum is over all inequivalent atoms j, with form factors f_j, within a (3×3) surface unit cell, and coordinates (x_j, y_j, z_j) are expressed as fractions of the dimensions of a bulk unit cell. Thus, intensity of reflection hkl is non-zero only when

$$(h, k) = (m, n) \text{ or } \left(m \pm \tfrac{1}{3}, n \pm \tfrac{1}{3}\right), \tag{6}$$

where m and n are both integers. Similarly, if only type-2 surface unit cells are present, intensities of only reflections hkl with

$$(h, k) = (m, n) \text{ or } \left(m \pm \tfrac{1}{3}, n \mp \tfrac{1}{3}\right), \tag{7}$$

where m and n are both integers, will be non-zero. Both types of surface unit cell must be present to give the observed diffraction pattern. The observation of a diffraction pattern of *p2mm* symmetry suggests the existence of four symmetrically related domains of $(\sqrt{3} \times \sqrt{3})$ unit cells. Possible arrangements of atoms in the equivalent (3×3) unit cells are illustrated in Fig. 6. For a multidomain system, where domain sizes are greater than the coherence length of the X-ray probe, measured intensities $\{I\}$ are incoherent averages of contributions from the various domains:

$$I = \frac{1}{D} \sum_{d=1}^{D} |b^{(d)} + s^{(d)}|^2. \tag{8}$$

Here D is the number of domains present, and $b^{(d)}$ and $s^{(d)}$ are respectively contributions to structure factors from the bulk and the surface layer of domain d. In particular, for the present case of four domains, in general,

$$I = \tfrac{1}{4}(|b^{(1)} + s^{(1)}|^2 + |b^{(2)} + s^{(2)}|^2 + |b^{(3)} + s^{(3)}|^2 + |b^{(4)} + s^{(4)}|^2). \tag{9}$$

The four domains have the same underlying bulk and therefore the same bulk contributions to structure factors: $b^{(1)} = b^{(2)} = b^{(3)} = b^{(4)} = b$, say. The four surface contributions form two *two-dimensional inversion pairs* (*i.e.* $x \rightarrow -x$, $y \rightarrow -y$), thus for in-plane reflections $(l = 0)$, using the notations introduced in Fig. 6, we have $s^{(4)} = s^{(1)*}$ for the two type-1 domains and $s^{(3)} = s^{(2)*}$ for the two type-2 domains. Thus, equation (9) becomes

$$I_{(hk0)} = \tfrac{1}{4}(|b + s^{(1)}|^2 + |b + s^{(2)}|^2 + |b + s^{(2)*}|^2 + |b + s^{(1)*}|^2). \tag{10}$$

For CTR reflections where $b \neq 0$, the contributions to intensities from the two type-1 domains are therefore not the same. Similarly for the two type-2 domains. However, it is important to note that, *e.g.* for in-plane SR reflections arising from type-1 domains, equation (10) reduces to

$$I_{(hk0)} = \tfrac{1}{4}(|s^{(1)}|^2 + |s^{(1)*}|^2) = \tfrac{1}{2}|s^{(1)}|^2 = \tfrac{1}{2}|s^{(4)}|^2. \tag{11}$$

The two type-1 domains therefore contribute equally to these intensities, and the autocorrelation function calculated using these intensities will give a map of interatomic vectors between X-ray scatterers in the surface region of both type-1 domains. Of course, a similar argument holds for the in-plane SR reflections from the type-2 domains. Fig. 7 depicts schematically the contributions of each of these types of domain to the observed in-plane reflections.

5. Unit-cell contents from 'in-plane' superstructure spot Patterson function

If a surface reconstructs so that the dimensions of its two-dimensional unit cell are larger than those of the bulk, non-zero diffraction intensities can be measured for certain

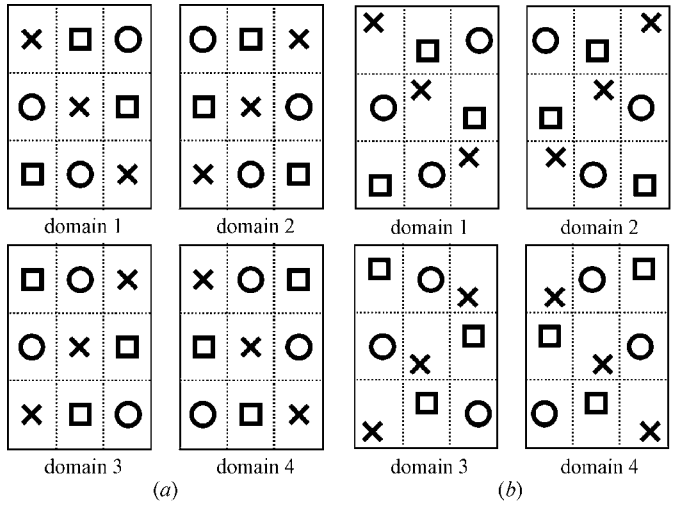

Figure 6
Examples to illustrate the need for four domains. In each case, crosses, squares and circles represent atoms of different species at different heights. Domains 1 and 4 are of type 1 and domains 2 and 3 are of type 2. Domains 1 and 2 are related by a 'vertical' mirror plane (in the plane of the paper), so are domains 3 and 4. Likewise, domains 1 and 3 are related by a 'horizontal' mirror plane and so are domains 2 and 4. These four domains are different in general and therefore all four are required to preserve *p2mm* symmetry. If domains 2 and 3 are identical, in which case domains 1 and 4 will also be identical, then only two domains are needed. (*a*) Atoms in one of the four high-symmetry (atop, hollow, long bridge or short bridge) sites, unless atoms represented by squares and circles are of the same species and are at the same height, the four domains are different. (*b*) Atoms in general locations.

momentum transfer vectors with non-integer values of either or both of the 'in-plane' Laue indices h and k [equation (3)]. In the simplest case in which the two-dimensional lattice vectors for the surface are $\alpha\mathbf{a}_1$ and $\beta\mathbf{a}_2$, where α and β are positive integers, and $\mathbf{a}_1$ and $\mathbf{a}_2$ are the two-dimensional lattice vectors for the bulk, non-zero diffraction intensities can be measured at

$$(h, k) = \left(\frac{m}{\alpha}, \frac{n}{\beta}\right), \tag{12}$$

where m and n are integers.

The inverse Fourier transform of the intensities of X-ray reflections produces a real-space autocorrelation function, known as a Patterson function, that reveals the magnitudes and directions of interatomic vectors. For a surface superstructure commensurate with the bulk structure, the set of momentum transfer vectors for which either or both in-plane Laue indices are non-integers are known as fractional order or *superstructure* reflections, $\{\mathbf{q}_{SS}\}$. The Patterson function

$$P(\mathbf{r}) = \frac{1}{N}\sum_{\mathbf{q}\in\mathbf{q}_{SS}} I_{\mathbf{q}} \exp(-2\pi i\mathbf{q}\cdot\mathbf{r}), \tag{13}$$

calculated from the intensities of only in-plane superstructure reflections, is of particular interest in SXRD as it has been suggested (see *e.g.* Bohr *et al.*, 1986) that this function may be able to identify in-plane interatomic vectors between X-ray scatterers in the surface region. If so, this would put constraints on, and thus reduce, the number of possible starting models of the surface layer in a conventional structure refinement. However, as we demonstrate below, even for relatively simple systems, such a Patterson map can be misleading. The positive octant of a three-dimensional Patterson map calculated from the data of just the superstructure reflections that arise from type-1 domains is shown in Fig. 8.

The first point to notice is that there is no strong intensity out of the plane parallel to the surface that passes through the origin (let us call it the $z = 0$ plane). This suggests that all surface interatomic vectors are coplanar and thus that the surface structure (*i.e.* that which differs from the bulk) lies in a single plane. This implies that all adatoms must be coplanar, and that any other deviations from the bulk structure must also be found in this plane. This rules out substrate reconstructions or relaxations distributed over more than one plane.

Within the $z = 0$ plane, the only two strong non-origin peaks are found corresponding to interatomic vectors $\mathbf{a}_1 + 2\mathbf{a}_2$ and $2\mathbf{a}_1 + \mathbf{a}_2$. Other than confirming the $(\sqrt{3} \times \sqrt{3})$ nature of the surface, this Patterson map does not seem to provide any new insights into the atomic arrangement of the surface layer. At first sight, this Patterson map seems to contradict the expected Sb adatom coverage. A coverage of $\theta_{Sb} \approx \frac{2}{3}$ would correspond to six Sb adatoms, or two parallel rows, per (3×3) surface unit cell. The two non-origin strong peaks correspond to the interatomic vectors *within* each row, but the interatomic vectors *between* the two rows are missing. As we point out below, the explanation is that, *regardless of the actual surface structure*, the $z = 0$ plane of a partial Patterson map calculated from just the data of the superstructure reflections cannot have a positive peak corresponding to any interatomic spacing equivalent to a two-dimensional bulk lattice vector unless that spacing also corresponds to a two-dimensional surface lattice vector.

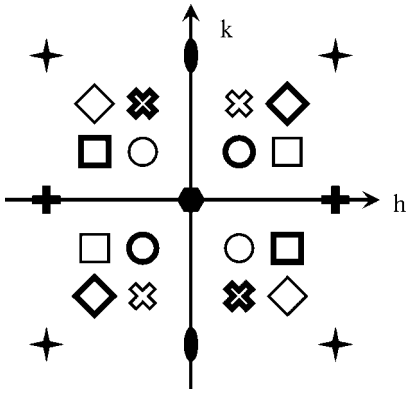

Figure 7
Schematic diagram showing how data are *symmetrized*. Owing to *p2mm* symmetry, only data for positive h and k need to be collected. (In practice, data were collected from all four quadrants to establish uncertainties in the measurements.) In the example here, four inequivalent superstructure reflections are measured (denoted by different unfilled geometric shapes: cross, diamond, circle and square). Intensities of reflections in the other quadrants can be obtained using symmetry. The four reflections denoted by the unfilled squares, for instance, have the same intensities. To calculate the autocorrelation function for, say, a type-1 domain, reflections denoted by unfilled shapes with thick outline are used. As can be seen in the schematic, all measured inequivalent superstructure reflections (*i.e.* cross, diamond, circle and square) are used.

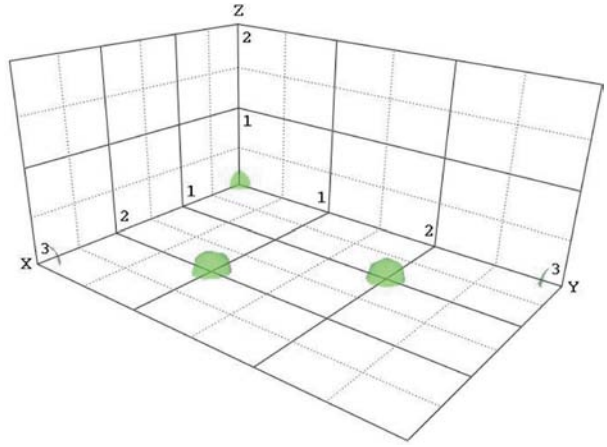

Figure 8
Positive octant of the three-dimensional partial Patterson function for the present data (calculated using only superstructure reflections that arise from type-1 surface domains) showing interatomic vectors in a volume occupied by $(3 \times 3 \times 2)$ bulk unit cells. Two strong non-origin peaks are observed at $(1, 2, 0)$ and $(2, 1, 0)$. Surprisingly, this map is consistent with either one row of Sb adatoms or two rows of Sb adatoms separated laterally by two-dimensional bulk lattice vectors [as discussed in the text, in the latter case, interatomic vectors corresponding to bulk lattice spacings cannot give rise to peaks at the expected locations $(1, 0, 0)$ or $(0, 1, 0)$].

Table 1
Conventional fitting results for the four high-symmetry models: hollow, atop, long bridge and short bridge.

Columns 2 and 3 list the fractional (x, y) coordinates, relative to a Au atom in the last Au layer, over which the Sb adatoms were held. The Sb adatoms were initially placed at half the height of a bulk unit cell above the last Au layer, which was taken to be unrelaxed. Changes in z positions (Å) of the Sb atoms and the last Au layer that minimized the reduced χ^2 are listed. All atoms in the models were assigned the Debye–Waller factor of bulk Au at RT.

	$Sb_1(\frac{x}{a_1}, \frac{y}{a_2})$	$Sb_2(\frac{x}{a_1}, \frac{y}{a_2})$	Δz_{Sb_1}	Δz_{Sb_2}	Δz_{Au}	χ^2
Hollow	$(\frac{1}{6}, \frac{1}{2}), (\frac{1}{2}, \frac{1}{6}), (\frac{5}{6}, \frac{5}{6})$	$(\frac{1}{6}, \frac{1}{6}), (\frac{1}{2}, \frac{5}{6}), (\frac{5}{6}, \frac{1}{2})$	−0.45	0.31	0.04	3.17
Atop	$(0, \frac{2}{3}), (\frac{1}{3}, \frac{1}{3}), (\frac{2}{3}, 0)$	$(0, \frac{1}{3}), (\frac{1}{3}, 0), (\frac{2}{3}, \frac{2}{3})$	0.16	2.80	−0.01	8.25
Long bridge	$(0, \frac{5}{6}), (\frac{1}{3}, \frac{1}{2}), (\frac{2}{3}, \frac{1}{6})$	$(0, \frac{1}{2}), (\frac{1}{3}, \frac{1}{6}), (\frac{2}{3}, \frac{5}{6})$	−0.09	2.5	−0.01	8.02
Short bridge	$(\frac{1}{6}, \frac{2}{3}), (\frac{1}{2}, \frac{1}{3}), (\frac{5}{6}, 0)$	$(\frac{1}{6}, \frac{1}{3}), (\frac{1}{2}, 0), (\frac{5}{6}, \frac{2}{3})$	−0.25	2.6	0.00	8.18

The proof of this statement follows from (13) and Friedel's law, which implies that $I_{\mathbf{q}} = I_{-\mathbf{q}}$, and we deduce that

$$P(x, y, 0) = \frac{1}{N} \sum_{(h,k)\in(h,k)_{SS}} J_{h,k} \cos(2\pi\{hx + ky\}), \qquad (14)$$

where $J_{h,k} = \sum_l I_{h,k,l}$. For Bragg reflections from a type-1 domain, the Laue indices (h, k) of the superstructure rods take the form $(m \pm \frac{1}{3}, n \pm \frac{1}{3})$, where m and n are integers (see Fig. 3), and hence the cosine term in equation (14) takes the form $\cos\{2\pi[(m \pm \frac{1}{3})x + (n \pm \frac{1}{3})y]\}$, which for integer values of the in-plane fractional coordinates x and y (two-dimensional bulk lattice vectors) reduces to $\cos[\frac{2\pi}{3}(x + y)]$ and is positive only if $x + y$ is a multiple of three, *e.g.* $(x, y) = (0, 0), (1, 2)$ or $(2, 1)$. The vectors joining the latter two points to the origin correspond to two-dimensional surface lattice vectors. This suggests that, of the set of bulk lattice vectors, only the surface lattice vectors may give rise to positive peaks in such a two-dimensional partial Patterson function *independent of the actual surface structure*.

It should be emphasized that these are not general limitations of the Patterson function, an established device in crystallography, but rather of the kind of partial Patterson function described here, calculated from the data of only the surface structure factors associated with SRs. (Those associated with the CTRs are not immediately accessible, since a CTR is formed by the interference between bulk and surface structure factors.)

Knowing that each (3×3) surface unit cell contains six Sb adatoms ($\theta_{Sb} \approx \frac{2}{3}$) forming two parallel rows, and that the two rows must be separated laterally by exactly a two-dimensional bulk lattice vector (a vector that cannot show up on the partial Patterson map), we proceed to refine by conventional means the four most 'obvious' trial models. In these models, Sb atoms are placed at half the height of a bulk unit cell (*i.e.* $\frac{1}{2}a_3$) above the last Au layer (taken to be unrelaxed), over the hollow, atop, long bridge or short bridge sites. All the atoms in the models are assigned the Debye–Waller factor of bulk Au at RT and only the vertical positions of the Sb adatoms and the first Au layer are allowed to vary to minimize the reduced χ^2. Results are summarized in Table 1. As expected, occupation of hollow sites is preferred. However, all χ^2 values are significantly higher than would be expected for a correct structural model. Since none of these 'obvious' models seem particularly promising, we turn to our direct method, which is described next.

6. Phase and amplitude recovery and diffraction image generation method

The aim of a direct method in X-ray diffraction is to remove the need for the initial inspired guess of a trial model. Rather, the aim is to deduce, directly from the measured data, an approximate electron density that suggests a structural model that can be refined rapidly by conventional means. An approximate representation of the surface electron density may be found from an inverse Fourier transform of the structure factors associated with this electron density. The amplitudes of these structure factors associated with the SRs are proportional to the square roots of the SR intensities, and are thus directly accessible to experiment. The complex surface structure factors associated with the CTRs form an interference pattern with the structure factors of the deeper bulk-like atomic layers. What is measurable is the resulting set of (real) intensities. Any attempt to recover directly the entire surface electron density would need to solve two problems: (1) to isolate the phase and amplitude scattering contributions of the surface structure factors to the CTR intensities, and (2) to determine the phases associated with the amplitudes of the SRs.

By *oversampling* the continuous diffraction patterns from non-periodic objects with respect to their Nyquist frequencies, Miao *et al.* (1999) were able to devise an algorithm that was able to find the *phases* associated with the diffraction amplitudes, which are directly accessible from experiment. The algorithm involves alternately satisfying constraints to the experimental data in reciprocal space and a support constraint in real space. Upon convergence, this algorithm yields the phases associated with the diffraction amplitudes in reciprocal space, and a 'diffraction image' of the object in real space. We take this approach one step further: although in the cases of the SRs we find the phases associated with measured diffraction intensities, as in the method of Miao *et al.*, our algorithm is able also to isolate *both* the *amplitudes* and *phases* of the surface structure factors contributing to the CTRs, hence the name phase and amplitude recovery and diffraction image generation method [1] (or PARADIGM, for short).

[1] Of course, in no way does our use of the term 'image' in this context imply a representation of the contents of any single unit cell. Rather, the term is used in the sense of Bragg (1939), in his description of the recovery of the average of the contents of a large number of unit cells from a diffraction pattern with the device he termed an 'X-ray microscope'.

A schematic diagram of the algorithm is illustrated in Fig. 9. This describes a set of repeated cycles between real-space operations on the left and reciprocal-space operations on the right. The cycles may be initiated at the first iteration ($n = 0$) with a flat distribution $\{u_j^{(0)}\}$ of the surface electron distribution (where the subscript j refers to a real space voxel). The coefficients $\{S_{\mathbf{q}}^{(n)}\} = \mathrm{FT}\{u_j^{(n)}\}$ of its Fourier transform at the nth iteration may be regarded as estimates $\{S_{\mathbf{q}}^{(n)}\}$ of the surface structure factors corresponding to scattering wavevectors $\mathbf{q}$ at the same iteration. Adding these to the corresponding structure factors $\{B_{\mathbf{q}}\}$ of the bulk, and taking the arguments of the resulting complex numbers give the estimated phases $\{\phi_{\mathbf{q}}^{(n)}\}$ of the corresponding total structure factors $\{F_{\mathbf{q}}^{(n)}\}$, whose amplitudes are constrained to be $c^{(n)}|F_{\mathbf{q}}^{\mathrm{obs}}|$, where $|F_{\mathbf{q}}^{\mathrm{obs}}|$ is the corresponding measured structure factor, and

$$c^{(n)} = \frac{\sum_{\mathbf{q}} |F_{\mathbf{q}}^{(n)}||F_{\mathbf{q}}^{\mathrm{obs}}|}{\sum_{\mathbf{q}} |F_{\mathbf{q}}^{\mathrm{obs}}|^2} \tag{15}$$

is a scaling factor found by the least-squares minimization of the difference between the observed and current estimate of calculated structure factors.

Revised estimates $\{T_{\mathbf{q}}^{(n)}\}$ of the surface structure factors may be found by subtracting from these estimates of the total structure factors the bulk structure factors (Marks, 1999; Saldin, Harder, Vogler *et al.*, 2001), *i.e.*

$$T_{\mathbf{q}}^{(n)} = c^{(n)}|F_{\mathbf{q}}^{\mathrm{obs}}| \exp\{i\phi_{\mathbf{q}}^{(n)}\} - B_{\mathbf{q}}. \tag{16}$$

An inverse Fourier transform of these quantities would give a new estimate

$$\{t_j^{(n)}\} = \mathrm{FT}^{-1}\{T_{\mathbf{q}}^{(n)}\} \tag{17}$$

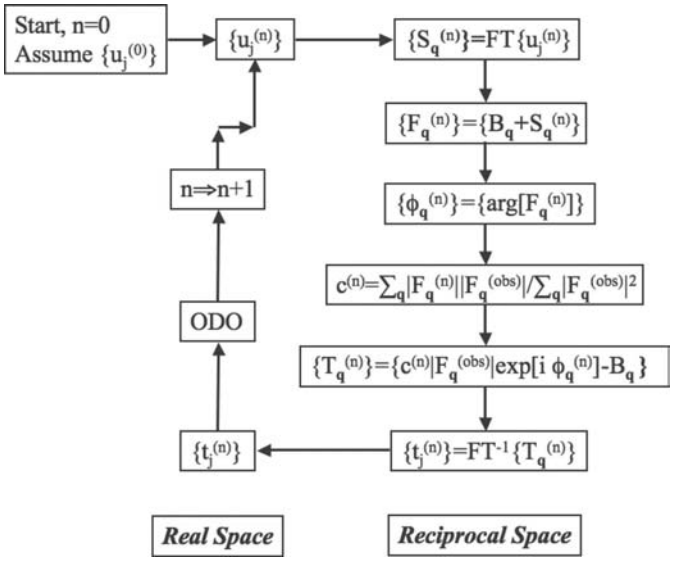

Figure 9
Flowchart of the PARADIGM for a single-domain surface. The indicated operations are performed on all elements of the sets of quantities enclosed by the braces. The individual elements of each set are characterized by the subscripts. The notation ODO represents the object domain operations described in the text. Other symbols are also defined in the text.

of the surface electron distribution that is constrained by the experimental data (bottom right of Fig. 9).

The next step is to apply a constraint in real space known as an *object domain operation* (ODO). Following Fienup (1978), we employ a constraint of compact support, in our case in the direction normal to the surface (the direction in which the data are oversampled). A solution to the determination of the extent of the support region from the experimental data alone for a general non-periodic object has been suggested by Marchesini *et al.* (2003). As a corollary, we estimated the height of the surface slab defining our region of compact support by taking the one-dimensional Fourier transform of the *intensity* of a SR of low values of in-plane Laue indices, h and k. This will give an estimate of the extent of the autocorrelation function of the surface electron density in the direction of $\mathbf{a}_3$, which will be about twice the height of the surface slab. Since the diffraction rods can be sampled at quite fine intervals along the rods, a Fourier transform of such data used to calculate $\{t_j^{(n)}\}$ will generally (*i.e.* if the phases are not correct) give non-zero values over a range of heights much larger than the physical height of the surface electron density. A real-space constraint may be imposed by defining a new estimate $\{u_j^{(n+1)}\}$ of the electron density at the next iteration by (Fienup, 1978)

$$u_j^{(n+1)} = \begin{cases} t_j^{(n)}, & j \notin \gamma \\ 0, & j \in \gamma, \end{cases} \tag{18}$$

where γ forms the set of grid points that lie in a region *not* expected to contain electron density. The next iteration of the algorithm consists of repeating the above steps but with $\{u_j^{(n+1)}\}$ substituted for $\{u_j^{(n)}\}$, and the iterations may be continued until successive estimates of the surface electron distribution $\{u\}$ do not differ appreciably. Since the process we have described forms an iteration cycle that is continued to self-consistency, it is relatively unimportant whether the starting point is a flat distribution of electron densities $\{u_j^{(0)}\}$ in real space or a random set of phases $\{\phi_{\mathbf{q}}^{(0)}\}$ in reciprocal space [equation (16)]. Independently of the starting point, the algorithm usually converged within a few tens of iterations to give a clean image showing concentrations of electron densities, which may be interpreted as a set of initial atom positions of a starting surface model for a subsequent conventional refinement.

The basic scheme above applies strictly only to single-domain systems. In equation (16) for instance, $B_{\mathbf{q}}$ can only be subtracted from the scaled $F_{\mathbf{q}}$ if they are both single-domain structure factors. When multiple domains are present, the measured quantity $|F^{\mathrm{obs}}|^2$ is an average over contributions from the domains.

For the system under study, we expect the domain sizes to be larger than the coherence length of the X-ray probe, and hence that the measured intensities are incoherent averages of contributions from all the domains [equation (8)]. The intensity contribution from one domain (say domain 1) at iteration n is therefore (Saldin *et al.*, 2002)

$$|f_{\mathbf{q}}^{(1,n)}|^2 = c^{(n)} D |F_{\mathbf{q}}^{\rm obs}|^2 - \sum_{d=2}^{D} |f_{\mathbf{q}}^{(d,n)}|^2, \tag{19}$$

where $|F_{\mathbf{q}}^{\rm obs}|^2$ is the measured intensity for scattering vector $\mathbf{q}$, $f_{\mathbf{q}}^{(d,n)} = b_{\mathbf{q}}^{(d)} + s_{\mathbf{q}}^{(d,n)}$ is the estimate at iteration n of the total structure factor from domain d, consisting of a sum over the corresponding bulk $b_{\mathbf{q}}^{(d)}$ and surface $s_{\mathbf{q}}^{(d,n)}$ structure factors, D is the number of domains and the scaling factor $c^{(n)}$ is defined by (15), with

$$|F_{\mathbf{q}}^{(n)}| = \left(\frac{1}{D} \sum_{d=1}^{D} |f_{\mathbf{q}}^{(d,n)}|^2 \right)^{1/2}. \tag{20}$$

Thus, equation (16) is replaced by

$$t_{\mathbf{q}}^{(1,n)} = |f_{\mathbf{q}}^{(1,n)}| \exp\{i\phi^{(1,n)}\} - b_{\mathbf{q}}^{(1)}. \tag{21}$$

Since, for symmetry-related domains, $f_{\mathbf{q}}^{(d,n)} = f_{\mathbf{q}'}^{(1,n)}$, where $\mathbf{q}$ and $\mathbf{q}'$ are related by symmetry, the current estimate of the set of complex amplitudes $\{f_{\mathbf{q}}^{(1,n)}\}$ will enable the calculation of the set $\{f_{\mathbf{q}}^{(d,n)}\}$ for each of the other domains d. Therefore, the current estimates of the structure-factor amplitudes $\{f_{\mathbf{q}}^{(1,n)}\}$ from domain 1 may be made consistent with the experimental data $\{|F_{\mathbf{q}}^{\rm obs}|\}$ *via* (19). The Fourier transform of the set of amplitudes $\{t_{\mathbf{q}}^{(1,n)}\}$ gives the current estimate of the surface electron distribution in a unit cell of domain 1. By this procedure (the flow chart in Fig. 10), it is possible to recover the electron distribution of a unit cell of any single domain even when multiple domains contribute to the measured diffraction intensities. Three orthogonal projections of isosurfaces of the electron density recovered in this case by the PARADIGM are shown in Fig. 11, together with dots that indicate the final positions of the adatoms deduced from a conventional refinement procedure (as described in the next section). The electron-density isosurfaces in the (*XY*) projection in a direction perpendicular to the surface suggest

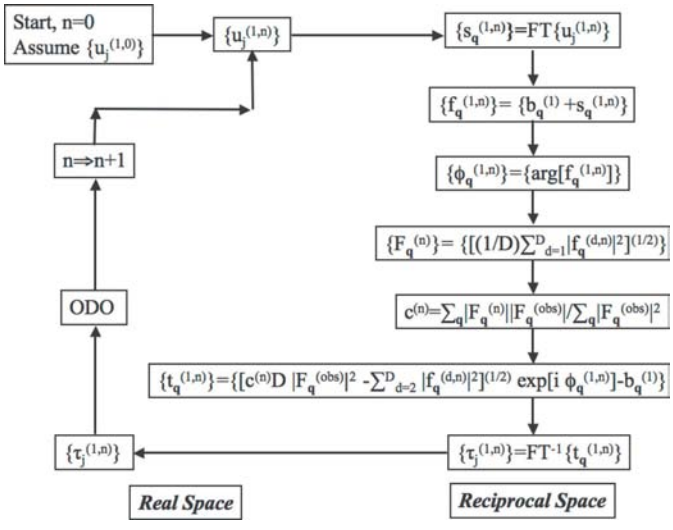

Figure 10
Same as Fig. 9 except for multiple incoherently scattering domains. The recovered electron distribution $\{\tau^{(1,n)}\}$ is that of domain 1. The other symbols are defined in the text.

that adatoms are adsorbed close to all hollow sites of the substrate. The isosurfaces also suggest that the adatoms form three distinguishable and repeating rows along diagonals parallel to a line connecting the top left to the bottom right of this projection. While the isosurfaces on the long diagonal in this panel seem to be closely tied to the exact hollow sites in their corresponding unit cells, the other two diagonals appear to consist of adatom rows slightly displaced *toward* each other. Since the Sb coverage is consistent with two diagonal rows of Sb out of every three, it might be supposed that the slightly displaced rows consist of Sb adatoms, and that the undisplaced row is one of Au adatoms.

Since, as we have already seen, a partial Patterson function of the kind in Fig. 8 is not expected to show up adatom–adatom vectors equal to bulk lattice vectors that are not also unit vectors of the superstructure (see also Lyman *et al.*, 2006), that partial Patterson function is entirely consistent with the above interpretation of the isosurface map from the PARADIGM.

Note also that, unlike the Patterson function, which is calculated from data of just SRs, which arise purely from surface scattering, and can thus reveal only interatomic vectors between adatoms, the PARADIGM operates on the data from both SRs and CTRs. Since the intensities of the latter rods are formed by the interference between bulk and surface scattering, the surface electron-density map from the PARADIGM has a spatial origin defined with respect to the substrate. One consequence of this difference is that, although the Patterson map of Fig. 8 is consistent with many different overlayer adsorption sites, the electron-density map of Fig. 11 clearly indicates hollow-site adsorption.

Furthermore, the PARADIGM also suggests approximate heights of the adatom rows above the outermost layer of the substrate. Indeed, the side (*XZ* and *YZ*) projections suggest that the adatoms lie approximately half a thickness of a bulk unit cell above the outermost substrate layer, in approximately the same relation of successive atomic planes in the bulk.

Sample CTRs and SRs simultaneously calculated from assumed bulk structure factors and from the surface electron density recovered by the PARADIGM are indicated by the open circles in Figs. 1 and 2, and are seen to be a reasonable fit to the experimental data, except for regions with low values of the Laue index l, affected by total external reflection not modeled by the PARADIGM, and/or other low-intensity portions of the rods.

7. Conventional structure refinement

The aim of the PARADIGM is to reveal an approximate electron density of the surface region. As with bulk X-ray crystallography (see *e.g.* Drenth, 1994), accurate values of structural parameters are still best found by the conventional refinement of an atomistic model based on the recovered electron density. We did this using the *ROD* program developed by Vlieg (2000). We took as a starting point a model of 2/3 ML of Sb adatoms and 1/3 ML of Au adatoms at half the height of a bulk unit cell above the outermost Au layer, and

Table 2
Conventional fitting results for the model suggested by the PARADIGM.

Surface atoms were initially placed at half the height of a bulk unit cell above the last Au layer, directly over the hollow sites. Changes in positions (Å) of the surface atoms and relaxation of the last Au layer that minimized the reduced χ^2 are listed. All atoms in the model were assigned the Debye–Waller factor of bulk Au at RT. The reduced χ^2 of the model (with restricted free parameters) is 2.35.

	Δx	Δy	Δz
Sb_1	−0.07	−0.17	−0.37
Sb_2	0.06	0.00	0.50
Au	0.01	0.08	−0.05
Au layer	N/A	N/A	0.12

Table 3
Conventional fitting results for the model suggested by the PARADIGM.

Parameters are the same as in the caption to Table 2, except that the Debye–Waller factors (Å^2) for the surface atoms and the Au atoms in the last layer are also allowed to vary. The reduced χ^2 for this model is 1.74.

	Δx	Δy	Δz	B
Sb_1	-0.16 ± 0.01	-0.19 ± 0.01	-0.29 ± 0.02	4.2 ± 0.2
Sb_2	0.05 ± 0.01	-0.01 ± 0.01	0.61 ± 0.02	10 ± 1
Au	-0.03 ± 0.01	0.03 ± 0.01	-0.05 ± 0.01	1.3 ± 0.1
Au layer	N/A	N/A	0.11 ± 0.01	1.1 ± 0.1

directly over the hollow sites. The Sb coverage of 2/3 implied by our results is both natural for a $(\sqrt{3} \times \sqrt{3})$ reconstruction and consistent with the value of 0.8 ± 0.15 ML we measured for the Sb/Au(110)–$(\sqrt{3} \times \sqrt{3})$R54.7° surfaces we prepared in the XPS chamber at the University of Wisconsin–Milwaukee. The positions of the adatoms were varied in all directions, subject to symmetry restrictions. The best fit model yielded a reduced χ^2 value of 2.35, much lower than that of the previous models. Details of the fit are summarized in Table 2.

An even lower reduced χ^2 of 1.74 is obtained if the adatoms and the Au atoms in the outermost bulk layer are allowed to have Debye–Waller factors different from the bulk Au atoms at RT. The elevated values of the Debye–Waller factors for the two Sb atoms in this model (Table 3) is somewhat troubling. However, allowing for partial occupancies of surface Au and Sb atoms reduces these Debye–Waller factors to lie within reasonable range, but with high error bars. The final reduced χ^2 value of 1.51 indicates that our final model (Table 4) is in very good agreement with the data, as is also evident from the sample calculated CTRs and SRs represented by solid lines in Figs. 1 and 2, respectively. The better agreement with the measured data for low values of l than the output of the PARADIGM is due to a correct modeling of total external reflection by the *ROD* program.

The relationship between the isosurfaces from the PARADIGM and the adatom positions deduced from this conventional refinement is also indicated in the various panels of Fig. 11. The red dots in these panels indicate the projections of the Au adatom positions, and the blue ones those of the Sb atoms. The isosurfaces of the *XY* projection of the top panel are seen to indicate lateral positions of the adatoms remarkably accurately, including a clear indication of a lateral pairing of neighboring Sb rows.

The slight buckling of alternate Sb rows suggested by the conventional structure refinement was not apparent from the electron-density isosurfaces from the PARADIGM, probably due to the reduced resolution of the data in the direction perpendicular to the surface (noted in §3).

8. Discussion

There have been several previous proposals for a direct method for SXRD. Rius and co-workers proposed a method

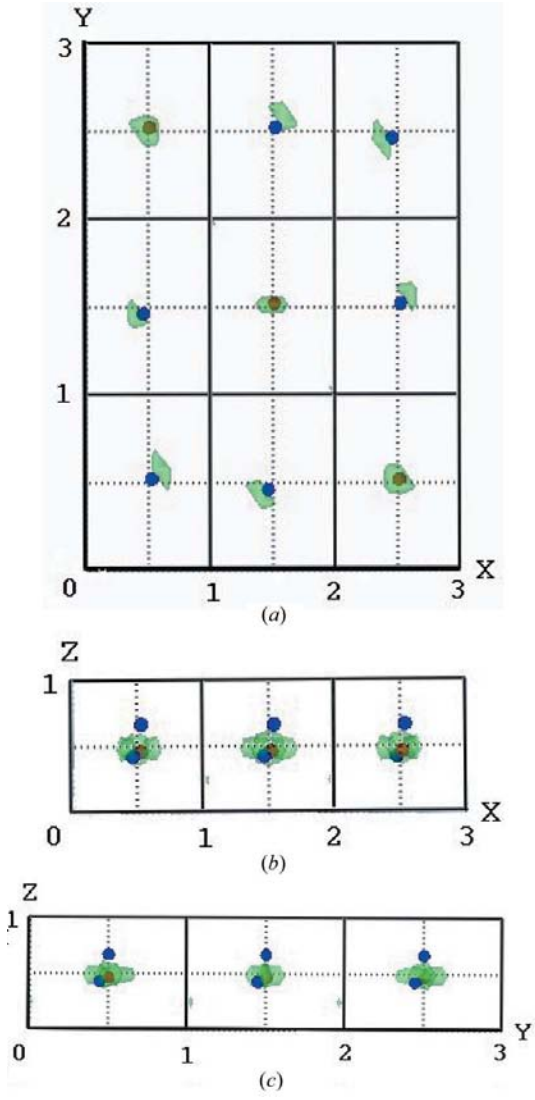

Figure 11
Three orthogonal projections of isosurfaces of the electron density of the surface unit cell of Sb/Au(110)–$(\sqrt{3} \times \sqrt{3})$R54.7°, as recovered by the PARADIGM. The x, y and z axes are measured in units of $a_1 = 2.88$, $a_2 = 4.07$ and $a_3 = 2.88$ Å, respectively, the defining vectors of a bulk unit cell. The accuracy of this electron-density map may be judged by comparisons with the projected positions of Au adatoms (red dots) and Sb adatoms (blue dots) as found by a final conventional structure refinement, starting from the atom locations suggested by the PARADIGM.

Table 4
Conventional fitting results for the model suggested by the PARADIGM.

The parameters are the same as in the caption to Table 2, except that the Debye–Waller factors (Å^2) for the surface atoms and the Au atoms in the outermost layer, as well as the occupancies of the surface atoms are allowed to vary. The reduced χ^2 for this model is 1.51.

	Δx	Δy	Δz	B	Occ.
Sb_1	-0.09 ± 0.01	-0.20 ± 0.01	-0.23 ± 0.02	1.1 ± 0.6	0.69 ± 0.05
Sb_2	0.10 ± 0.01	0.03 ± 0.01	0.47 ± 0.01	0.67 ± 0.51	0.61 ± 0.02
Au	0.06 ± 0.01	0.04 ± 0.01	-0.12 ± 0.01	1.4 ± 0.1	0.96 ± 0.01
Au layer	N/A	N/A	0.10 ± 0.01	1.0 ± 0.1	N/A

(Rius *et al.*, 1996) that considers only the intensities of the SRs. They neglect the data in the CTRs where the surface contributions are inherently combined with contributions from the bulk. They noted that, even if the SR amplitudes could be phased, their inverse Fourier transform would generate not the desired full surface electron density but rather the *difference* electron density, that is the difference between the true surface electron density and the average surface electron density (from the value of the true surface electron density averaged over each bulk unit cell). This difference electron density can be positive or negative. Thus, traditional direct methods stemming from Sayre's equations (Sayre, 1952) that rely on the similarity of an electron-density distribution (regarded as a sum of atomic contributions) to its square are no longer applicable. However, Rius *et al.* pointed out that a difference electron-density distribution may be regarded as similar to its cube. Unlike Sayre's equations, which relate a structure factor to sums of products of two other structure factors, this leads to equations that relate a structure factor to sums of products of three other structure factors. Nevertheless, these authors were able to show that even these more complicated equations may be solved numerically to phase at least the in-plane parts of the SRs to yield the projected difference electron density of the surface. In favorable cases (where the superstructure has few interatomic vectors in common with those of the underlying bulk and for flat superstructures parallel to the surface), this has enabled the solution of quite complex superstructures (Torrelles *et al.*, 1998).

A different approach has been proposed by Yacoby and coworkers (Yacoby *et al.*, 2000). There are two variants of their method, termed COBRA (or coherent Bragg rod analysis). One requires the evaporation of a thin gold film onto a sample in order to create an extra interference condition to determine the phase variation along a CTR. The other relies on the relatively slower variation of the phase of a surface structure factor than that of the underlying substrate to give rise to pairs of simultaneous equations that may be solved for the complex structure factors of the unknown surface region. Since both variants of this method require interference of the surface scattering amplitudes with those of the known substrate, they can operate only on the CTR data. Consequently, only those surface structure factors that contribute to the CTRs may be found, and hence this method may only strictly determine the average surface structure. We note, however, that those workers claim to be able (in favorable cases) to unravel the unfolded surface structure using additional considerations such as the bulk structure of an epitaxic film (Sowwan *et al.*, 2002).

An ideal direct method for surface crystallography would use the information in both CTRs and SRs and would be able to recover the full three-dimensional structure of a surface unit cell. Such a scheme has been proposed by Marks (1999) that 'exploits the existence of a support constraint normal to the surface, and couples the concepts of projections, operators, and sets used in the image reconstruction literature with statistical operators used in direct methods'. It also assumes that 'the scattering comes from atoms', and has helped determine the structure of NiO(111)–$p(2 \times 2)$ (Erdman *et al.*, 2000) and the $c(8 \times 2)$ reconstructions of InSb–, InAs–, and GaAs–(001) surfaces (Kumpf *et al.*, 2001).

The PARADIGM algorithm described in this paper likewise recovers the three-dimensional electron density of a complete surface unit cell from the data of both 'in-plane' and 'out-of-plane' CTRs and SRs by finding the complete surface structure factors (amplitude and phase) contributing to both. Since the aim is to recover the electron density rather than atomic positions, it does not impose an atomicity constraint. Furthermore, in the case of a multidomain surface structure, where the domains are related by symmetry operators of the underlying substrate, it is capable of determining the full surface electron density of a single domain from the diffraction data, as we have demonstrated here. After extensive testing on simulated SXRD data (Saldin, Harder, Shneerson & Moritz, 2001; Saldin, Harder, Vogler *et al.*, 2001; Saldin *et al.*, 2002), the method has now been successfully applied to at least three sets of measured experimental data (Lyman *et al.*, 2005, 2006, and the present paper) leading to the solution of unknown surface phases of Sb/Au(110) in the latter two cases.

9. Conclusions

We have described a scheme, the phase and amplitude recovery and diffraction image generation method (PARADIGM) for generating directly an image of the electron density of a surface unit cell from measured surface X-ray diffraction (SXRD) data. We have described an application of this method to determine the structure of the Sb/Au(110)–$(\sqrt{3} \times \sqrt{3})$R54.7° surface. This system provides an instructive illustration of a case where a partial Patterson function (calculated in the usual way from the Fourier transform of the in-plane SRs) is not very helpful in suggesting a useful starting structure for conventional refinement. The $(\sqrt{3} \times \sqrt{3})$ symmetry of the system demands that any real-space features

of the surface unit cell (*e.g.* adatoms) line up to form rows parallel to one of the two diagonals of the truncated bulk lattice of Au(110). The Patterson function suggests only that there may be one, two or three such rows separated laterally by two-dimensional unit vectors of this truncated bulk lattice.

Much more detailed information of the entire three-dimensional structure of the surface unit cell is revealed by our direct method. Although the known Sb coverage of about $\frac{2}{3}$ may suggest an Sb adatom structure of two parallel diagonal rows of Sb atoms in each (3×3) surface unit cell, the direct method yields a very clean electron-density map of three parallel diagonal rows of atoms per (3×3) surface unit cell, with the adatoms located near the hollow sites of the underlying bulk lattice. Given the coverage of Sb, one of the three rows of atoms was interpreted to consist of Au adatoms, the other two Sb ones. A conventional structure refinement of this model did indeed give by far the best fit with the experimental data.

Following on the heels of our recent determinations from experimental data of the structures of clean Au(110)–(2×1) (Lyman *et al.*, 2005), and of Sb/Au(110)–$c(2 \times 2)$ (Lyman *et al.*, 2006) by the same method, the latest success of our scheme is an encouraging indication of its potential as a general, routine, reliable and rapid starting point for the subsequent refinement of surface structures by conventional model-based refinement methods (*e.g.* Vlieg, 2000).

We acknowledge support for this work from the US DOE under grant number DE-FG02-06ER46277. One of us (SSP) received partial support from the US NSF *via* the MRSEC at the University of Wisconsin–Madison. Another (DKS) wishes to thank Professor Wolfgang Moritz for introducing him to the field of surface X-ray diffraction and for stimulating discussions on direct methods.

References

Andrews, S. R. & Cowley, R. A. (1985). *J. Phys. C*, **18**, 6427–6439.
Blow, D. M. & Crick, F. H. C. (1959). *Acta Cryst.* **12**, 794–802.
Bohr, J., Feidenhans'l, R., Nielsen, M., Toney, M., Johnson, R. L. & Robinson, I. K. (1986). *Phys. Rev. Lett.* **56**, 2878–2881.
Bragg, W. L. (1939). *Nature (London)*, **143**, 678.
Chevalier, P.-Y. (1989). *Thermochim. Acta*, **155**, 211–225.
Collins, D. M. (1982). *Nature (London)*, **298**, 49–51.
Drenth, J. (1994). *Principles of Protein X-ray Crystallography*. New York: Springer-Verlag.
Erdman, N., Warschkow, O., Ellis, D. E. & Marks, L. D. (2000). *Surf. Sci.* **470**, 1–14.
Fienup, J. R. (1978). *Opt. Lett.* **3**, 27–29.
Giacovazzo, C. (1980). *Direct Methods in Crystallography*. London: Academic Press.
Gibbs, D., Ocko, B. M., Zehner, D. M. & Mochrie, S. G. J. (1990). *Phys. Rev. B*, **42**, 7330–7344.
Green, D. W., Ingram, V. M. & Perutz, M. F. (1954). *Proc. R. Soc. London Ser A*, **225**, 287–307.
Hendrickson, W. A. (1991). *Science*, **254**, 51–58.
Keane, D. T., Bancel, P. A., Jordan-Sweet, J. L., Held, G. A., Mak, A. & Birgeneau, R. J. (1991). *Surf. Sci.* **250**, 8–16.
Kumpf, C., Marks, L. D., Ellis, D., Smilgies, D., Landemark, E., Nielsen, M., Feidenhans'l, R., Zegenhagen, J., Bunk, O., Zeysing, J. H., Su, Y. & Johnson, R. L. (2001). *Phys. Rev. Lett.* **86**, 3586–3589.
Leahy, D. J., Hendrickson, W. A., Aukhil, I. & Erikson, H. P. (1992). *Science*, **258**, 987–991.
Lyman, P. F., Shneerson, V. L., Fung, R., Harder, R. J., Lu, E. D., Parihar, S. S. & Saldin, D. K. (2005). *Phys. Rev. B*, **71**, 081402(R).
Lyman, P. F., Shneerson, V. L., Fung, R., Parihar, S. S., Johnson-Steigelman, H. T., Lu, E. D. & Saldin, D. K. (2006). *Surf. Sci.* **600**, 424–435.
Marchesini, S., He, H., Chapman, H. N., Hau-Riege, S. P., Noy, A., Howells, M. R., Weierstall, U. & Spence, J. C. H. (2003). *Phys. Rev. B*, **68**, 140101(R).
Marks, L. D. (1999). *Phys. Rev. B*, **60**, 2771–2780.
Miao, J., Charalambous, P., Kirz, J. & Sayre, D. (1999). *Nature (London)*, **400**, 342–344.
Millane, R. P. (1990). *J. Opt. Soc. Am. A*, **3**, 394.
Moffat, W. G. (1986). *The Handbook of Binary Phase Diagrams*. Schenectady: Genium.
Moritz, W. & Wolf, D. (1979). *Surf. Sci.* **88**, L29-L34.
Oszlányi, G. & Sütő, A. (2004). *Acta Cryst.* A**60**, 134–161.
Rius, J., Miravittles, C. & Allmann, R. (1996). *Acta Cryst.* A**52**, 634–639.
Robinson, I. K. (1986). *Phys. Rev. B*, **33**, 3830–3836.
Rossmann, M. G. & Blow, D. M. (1962). *Acta Cryst*. **15**, 24–31.
Saldin, D. K., Harder, R. J., Shneerson, V. L. & Moritz, W. (2001). *J. Phys. Condens. Matter*, **13**, 10689–10707.
Saldin, D. K., Harder, R. J., Shneerson, V. L. & Moritz, W. (2002). *J. Phys. Condens. Matter*, **14**, 4087–4100.
Saldin, D. K., Harder, R. J., Vogler, H., Moritz, W. & Robinson, I. K. (2001). *Comput. Phys. Commun.* **137**, 12–24.
Sayre, D. (1952). *Acta Cryst.* **5**, 60–65.
Seah, M. P. (1983). In *Practical Surface Analysis by Auger and X-ray Photoelectron Spectroscopy*, edited by D. Briggs & M. P. Seah. New York: John Wiley and Sons.
Sowwan, M., Yacoby, Y., Pitney, J., MacHarrie, R., Hong, M., Cross, J., Walko, D. A., Clarke, R., Pindak, R. & Stern, E. A. (2002). *Phys. Rev. B*, **66**, 205311.
Sprösser, J., Salanon, B. & Lapujoulade, J. (1991). *Europhys. Lett.* **16**, 283–288.
Torrelles, X., Rius, J., Boscherini, F., Heun, S., Mueller, B. H., Ferrer, S., Alvarez, J. & Miravitlles, C. (1998). *Phys. Rev. B*, **57**, R4281–R4284.
Vlieg, E. (1997). *J. Appl. Cryst.* **30**, 532–543.
Vlieg, E. (2000). *J. Appl. Cryst.* **33**, 401–405.
Wood, E. A. (1964). *J. Appl. Phys.* **35**, 1306–1312.
Woolfson, M. M. (1961). *Direct Methods in Crystallography*. Oxford University Press.
Yacoby, Y., Pindak, R., MacHarrie, R., Pfeiffer, L., Berman, L. & Clarke, R. (2000). *J. Phys. Condens Matter*, **12**, 3929–3938.